JOURNAL OF BACTERIOLOGY, Oct. 1986, p. 309–317
0021-9193/86/100309-09$02.00/0

Vol. 168, No. 1

Three-Dimensional Structure of the Tetragonal Surface Layer of *Sporosarcina ureae*

HARALD ENGELHARDT,[1]* W. OWEN SAXTON,[2] AND WOLFGANG BAUMEISTER[1]

Max-Planck-Institut für Biochemie, D-8033 Martinsried, Federal Republic of Germany,[1] and Department of Metallurgy and Material Science, University of Cambridge, Cambridge CB2 3RQ, England[2]

Received 1 April 1986/Accepted 30 June 1986

The three-dimensional structure of the regular surface layer of *Sporosarcina ureae* has been determined to a resolution of 1.7 nm by electron microscopy and image reconstruction. The S-layer has p4 symmetry, a lattice constant of 12.9 nm, and a minimum thickness of 6.6 nm. The reconstruction reveals a distinct domain structure: a massive core, arms connecting adjacent unit cells, and spurs which make contact at the subsidiary fourfold symmetry axes. In the *z*-direction the domains appear to be arranged in three planes, creating two entirely different surface reliefs. The S-layer has a complex pattern of pores and gaps that are 2 to 3 nm wide. In addition, the secondary-structure composition has been determined by infrared spectroscopy: about 35% of the polypeptide appears to have a β-structure conformation.

Regular surface layers (S-layers) have been found to be cell envelope components of many bacteria in almost all phylogenetic branches of both eubacteria and archaebacteria (31). They represent the border between the bacterial cell and the surrounding environment, unless the surface is coated by a dense heteropolysaccharide capsule. The functions attributed to S-layers are related to their exposed location; however, information on functional aspects is still rather scarce (31), and S-layers are probably multifunctional, especially since they may be associated with different components of the cell envelope (underlying membrane or peptidoglycan) (W. Baumeister and H. Engelhardt, *In* J. R. Harris and R. W. Horne (ed.), *Electron Microscopy of Proteins*, vol. 6, in press). Most information on S-layers has been accumulated by structural investigations using electron microscopy and image processing. Three-dimensional (3-D) reconstructions of regular layers of some unrelated bacteria (S_{AB} values of <0.3) have been completed, and these appear to have very different domain structures. The species that have been investigated are *Bacteroides buccae* (30), "*Synechocystis*" sp. (20), *Chlamydia trachomatis* (10), *Pseudomonas acidovorans* (9), *Deinococcus radiodurans* (2), the archaebacterium *Sulfolobus acidocaldarius* (12), and the regular cell sheath of *Methanospirillum hungatii* (29).

Sporosarcina ureae is a member of the classical gram-positive bacteria, closely related to *Bacillus pasteurii* and *Bacillus sphaericus* (14, 24). *S. ureae* possesses a tetragonal S-layer (3, 5) resembling the "T-layer" of *B. sphaericus* (1, 23), from which a 3-D reconstruction has also been recently completed (22). The complex multidomain structure of the *S. ureae* layer underlines the value and necessity of 3-D studies in order to compare the topology of S-layers adequately. Knowledge on the 3-D structure is a prerequisite for understanding the interactions between the S-layer, the environment, and the associated cell wall component. It was already clear from the earlier studies that the two surfaces of the *S. ureae* layer must be different (5, 33).

The 3-D reconstruction was obtained using the new real space/Fourier space approach (27) combining correlation averaging and conventional methods of 3-D reconstruction in Fourier space. High tilting yielded a nearly isotropic resolution with information extending to 1.7 nm. We describe here the 3-D structure as determined from negatively stained preparations and present some infrared (IR) spectroscopic data on the secondary structure of the S-layer protein.

MATERIALS AND METHODS

Cell cultivation and preparation. *S. ureae* ATCC 13881 was cultivated aerobically at 30°C in a medium (pH 8.0) containing 10 g of tryptone, 1 g of yeast extract, 1.1 g of glucose, and 0.02 mol of sodium phosphate per liter. The cells were harvested in the late-logarithmic-growth phase and then washed twice with a buffer solution (50 mM sodium phosphate, pH 7.8, 1 mM $MgCl_2$). The cells were resuspended in the same buffer solution and disintegrated in a cell mill at 4°C with glass beads of 0.1 to 0.11 mm diameter. Unbroken bacteria were removed by differential centrifugation, and the cell envelope fragments were suspended in buffer. Membranes were solubilized by treatment with 1% Triton X-100, and the cell walls were washed repeatedly. For solubilizing the peptidoglycan, lysozyme (0.1 mg/ml) was added, and the samples were then incubated for several hours at 30°C. The S-layer preparation was repeatedly washed, resuspended in small amounts of buffer containing 0.02% NaN_3, and stored at 4°C.

Electron microscopy. The S-layer preparation was suspended in distilled water and the layers adsorbed onto carbon-coated copper grids made hydrophilic by glow discharge. The preparations were negatively stained with 1.5% sodium phosphotungstate, pH 6.8, with 0.015% glucose added to promote homogeneous staining. Electron microscopy was performed using a Philips EM420 microscope equipped with the unlimited tilt specimen holder of Chalcroft and Davey (8). Micrographs were taken at 80 kV at a magnification of ×36,000. Sixteen images were recorded starting and finishing the series with untilted micrographs. Nominal tilts from 78.5° to 9.5° with unequal increments were applied according to the scheme of Saxton et al. (27).

The lattice constant of the S-layer was determined by electron diffraction according to a method described previously (17) using the diffraction rings of crystalline water for internal calibration.

* Corresponding author.

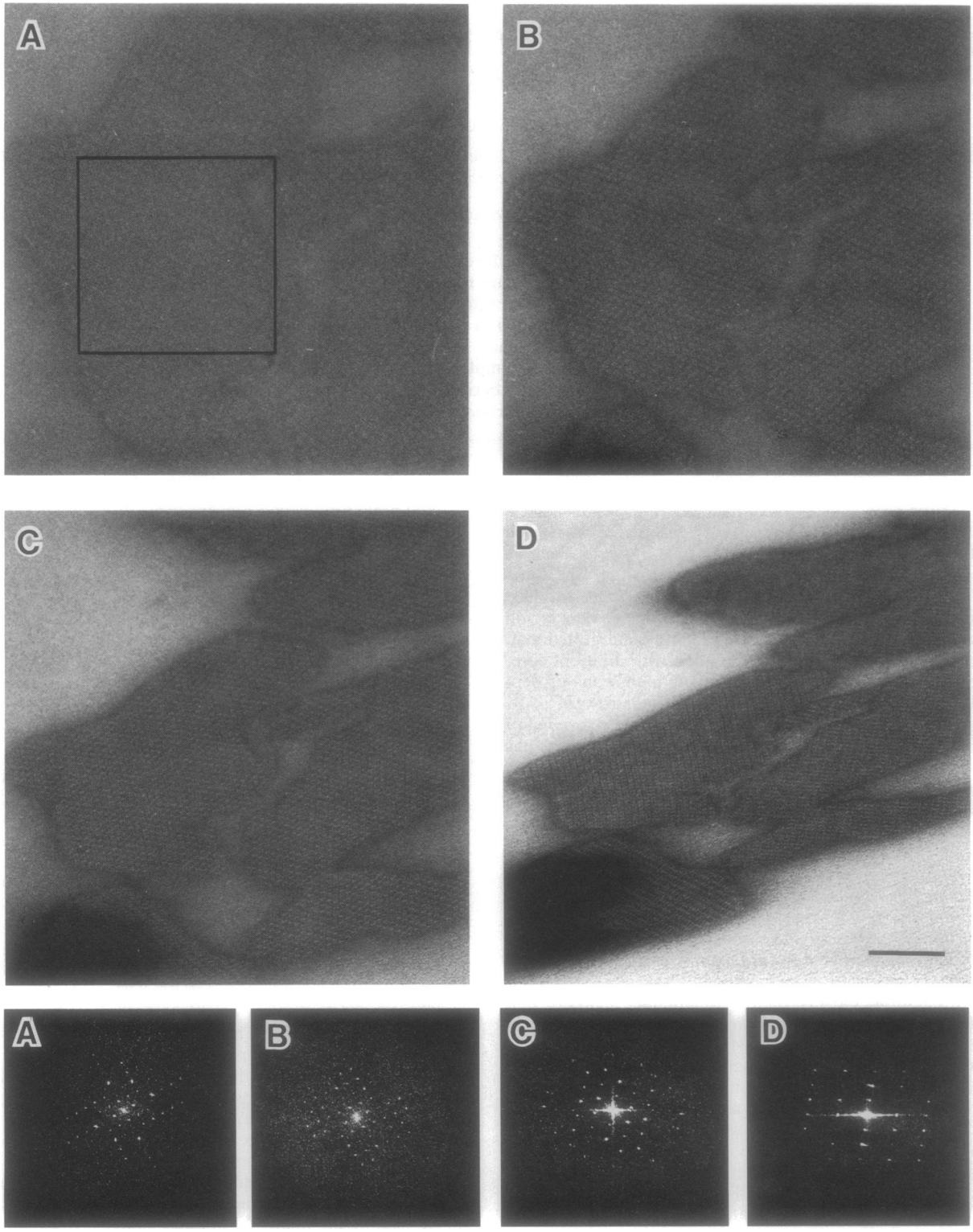

FIG. 1. Electron micrographs of the negatively stained S-layer of *S. ureae* and the corresponding diffractograms calculated from the digitized areas. The tilt angles were −4° (A), 47° (B), 63° (C), and 75° (D). The boxed area, containing about 550 unit cells, and corresponding areas of the tilted projections were selected for image processing. Bar, 100 nm.

Image processing. The micrographs were preselected using optical diffractometry. Two series of comparable quality showing opposite handedness in the optical diffractograms were digitized in arrays of 512 points square at an interval of 20 μm, corresponding to 0.59 nm at the specimen level.

The 3-D reconstruction was obtained using the hybrid real space/Fourier space method (27); average unit cells were obtained by correlation averaging (26). In view of the high focus gradient in high-tilt images, averaging was restricted to strips parallel to the tilt axis. The base vectors and the nominal-tilt angles were applied to a least-squares fitting program to determine the correct tilt angles, the specimen inclination, and the tilt axis azimuth. The offset was −3.7°, and the highest-tilt angle was thus 74.8°; the specimen inclination proved to be insignificant (<0.1°). The unit cells were extracted, aligned with each other, and normalized according to procedures described in detail previously (27). The lattice lines were fitted using the method of Shaw (28) as modified by Baumeister et al. (2); the lattice lines of higher orders were subsequently smoothed by hand if necessary. The extent of the lines was chosen to give a layer spacing of 0.15 nm. A 3-D model was obtained from the density distributions by applying suitable thresholding to each density layer. 3-D representations were created by a computer surface-shading program providing views of the reconstruction solid (25).

Surface relief reconstruction. Rapidly frozen cells were deep etched for 2 min at −100°C in a Balzers 360 freeze-etching machine and unidirectionally shadowed with ≈0.5-nm Ta/W at 45° and subsequently with about 15-nm carbon at normal incidence. Micrographs of the replica were digitized and subjected to correlation averaging as described above. Surface relief reconstruction was performed according to the method described in detail previously (18; W. Baumeister, R. Guckenberger, H. Engelhardt, and C. L. F. Woodcock, Ann. N.Y. Acad. Sci., in press) starting with unit cells extracted from correlation averages.

Attenuated total reflection IR spectroscopy. IR measurements of the S-layer were performed using the attenuated total reflection technique. The spectra were recorded with a Perkin Elmer 325 IR spectrometer as described in detail elsewhere (21). Datum points were obtained at increments of 0.714 cm^{-1} in the range of 2,000 to 1,000 cm^{-1}. The amide I and II bands (1,720 to 1,480 cm^{-1}) were subjected to band shape analysis for assessing the β-structure content of the S-layer protein. For this purpose a computer program based on the least-squares method of Fraser and Suzuki (16) was used. Input values for the positions, the half-widths, and the amplitudes of the expected bands were estimated according to the strategy outlined elsewhere (B. Kleffel, Diploma thesis, University of Düsseldorf, Düsseldorf, Federal Republic of Germany, 1980).

RESULTS

Assessment of data. The S-layer of *S. ureae* has p4 symmetry with a clear handedness visible in the optical diffractograms (3, 33). The images of the tilted specimen consistently contained information out to a crystallographic resolution of 2.1 nm, corresponding to the sixth diffraction order of the untilted projection (Fig. 1). Correlation averaging provided a resolution of 1.7 nm in the x,y-plane as assessed by the radial correlation function. The Fourier space is densely filled to 2 nm and more sparsely but significantly filled to 1.7 nm (Fig. 2). A comparison of the first and last micrograph of the tilt series indicated that radiation damage was not affecting the results; the power spectra and the resolution assessment curves are almost identical in the significant parts. Due to high tilting, only the first two lattice lines (corresponding to the lines 1,0 and 1,1) are incompletely covered (Fig. 2). The quality of the lattice line data obtained is illustrated by the examples shown in Fig. 3, together with the computer-fitted curves.

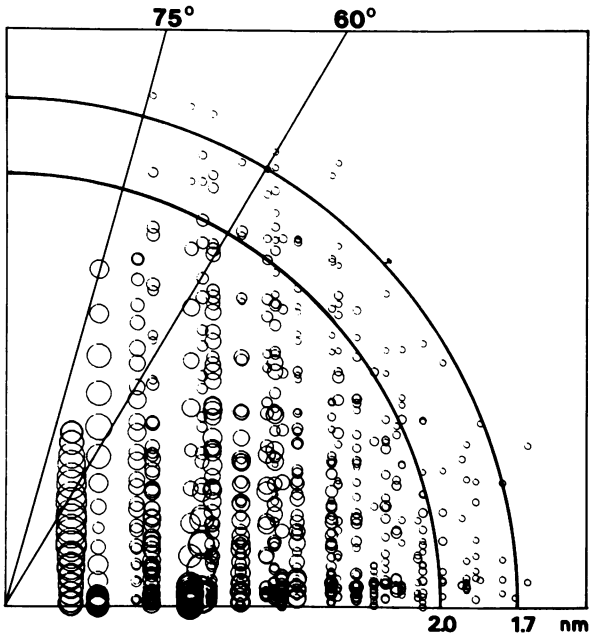

FIG. 2. Distribution of data in Fourier space. The ordinate corresponds to the z^*-axis and the abscissa to the r^*-axis ($r^{*2} = x^{*2} + y^{*2}$), respectively. The area enclosed by each circle is proportional to the modulus of the corresponding Fourier coefficient. Only data greater than 3.5% of the strongest coefficient are displayed. The curves indicate resolution spheres at 2 and 1.7 nm, and the lines indicate the missing data if tilting is restricted to 60°.

The consistency of the reconstruction with the original data was judged by comparing averages of the tilted images with corresponding projections through the 3-D reconstruction. Thresholding during the course of model building was performed using the following constraints: (i) the extent of the structure in the z-direction (i.e., perpendicular to the layer plane) as judged from the contrast variation curve, (ii) the steepest density gradients in the z-slices (i.e., horizontal sections), and (iii) the correspondence between the original averages and appropriate projections through the thresholded 3-D reconstructions. Some of the averages and the corresponding projections are shown in Fig. 4. The thresholded images appear to be somewhat fainter since only 70% of the expected volume is included.

Description of the structure. The tetragonal unit cell has a lattice constant of 12.9 nm, which is in agreement with earlier reports (3, 33). In projection it shows a characteristic substructure (Fig. 4 and 5): a massive core at the (major) fourfold symmetry axes, i.e., the major tetramer according to the nomenclature of Aebi et al. (1), arms connecting adjacent unit cells via the twofold symmetry axes, and spurs connecting corresponding substructures of neighboring unit cells at the subsidiary fourfold symmetry axes (minor tetramer). The horizontal and vertical sections through the 3-D reconstruction (Fig. 5 and 6) illustrate the arrangement

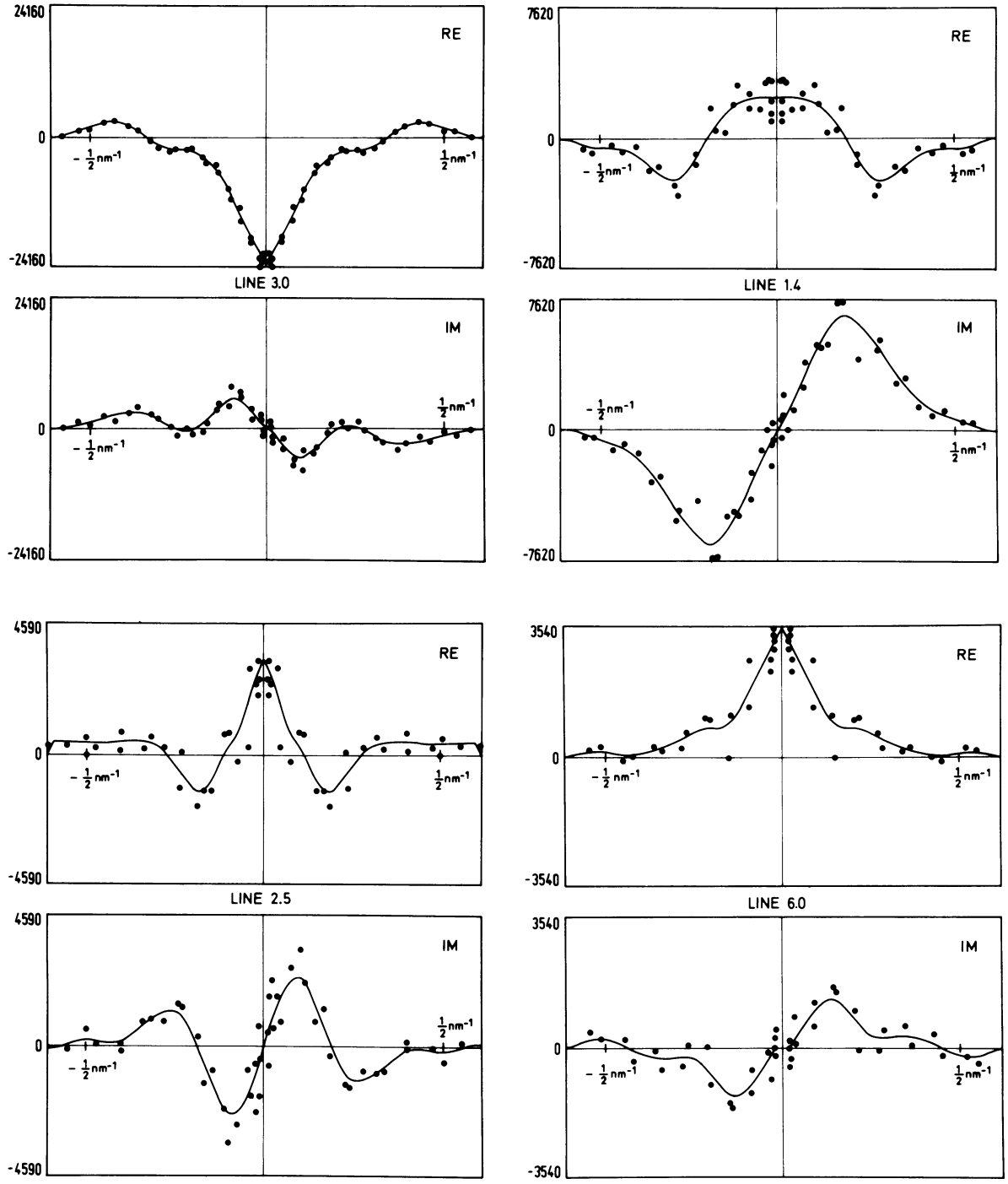

FIG. 3. Selected lattice lines (indices given) presented in real (amplitudes) and imaginary (phases) form. The continuous lattice lines, from which resampled data were drawn, were fitted by an automatic procedure. The resolution of 2 nm is indicated.

of the core, arms, and spurs, emanating from the underside of the arms, in three planes in the z-direction. The orientation of the S-layer with respect to the cell was determined by surface relief reconstruction of freeze-etched and heavy-metal-shadowed cells. The structure of the relief of the outer surface in Fig. 7 corresponds to the smooth surface aspect (Fig. 5A and 8); thus in turn, the side showing the massive core in the 3-D reconstruction can unambiguously be assigned to the inner surface of the S-layer. A corresponding orientation was proposed by Stewart and Beveridge (33) based on micrographs of sectioned material.

The core is split into two parts, a massive tetramer at the inner surface and a lighter tetramer at the outer face; both tetramers are rotated 45° with respect to each other. While the other structural domains are clearly connected, the small tetramer shows only a weak connectivity, suggesting that this part may represent a flexible feature of the S-layer. The core encloses a large cavity (maximum diameter, 4 nm) with

an apparently smaller opening (approximate diameter, 2.5 nm) at the outer surface. The pore appears to be closed at the inner side, possibly due to distortions induced by some flattening of the core upon adsorption to the carbon film (Fig. 5).

If the reconstruction is performed with a restricted range of tilts (up to 58.5° only), the structure changes remarkably. The reconstruction is apparently thicker, the mass distribution at the subsidiary fourfold symmetry axis is altered, and significant "mass" appears in the pore, closing it entirely.

Another 3-D reconstruction of the S-layer oriented with the outer surface towards the carbon support (data not shown), revealed an unflattened core (but the pore was still closed, tilts being available to 70° only); the spurs, which in this orientation are touching the carbon film, show no obvious distortions, indicating a rigid structure. The domain disposition was identical in the two reconstructions; hence we conclude that our 3-D structure does not suffer from gross artifacts due to effects such as surface denaturation or partial staining. Low stain levels tend to emphasize one of the two surface aspects and have been exploited by Steward and Beveridge (33) in order to obtain a rough idea of the 3-D organization of the layer. We have not observed one-sided staining patterns in our preparations, which would clearly be undesirable for a complete 3-D reconstruction.

The thickness of the S-layer is about 6.6 nm, as assessed from the contrast-variation curve drawn from the reconstructed z-slices. The 3-D model, presented as computer-generated views (Fig. 8), provides an impression of the two sides. The surface showing the massive core has a rough appearance with deep "valleys" (ca. 4.5 nm) at the subsidiary fourfold symmetry axes; the outer surface (smooth) shows numerous gaps and holes (2 to 3 nm wide), but all domains extend to about the same level. The model in Fig. 8 fills about 70% of the expected volume, based on a molecular weight estimate for the monomer of 115 kilodaltons (kDa) (obtained from lithium dodecyl sulfate-polyacrylamide gel electrophoresis) and a specific protein density of 1.37 g/cm^3. The apparent molecular weight corresponds to earlier results (3) and was confirmed by mass determination (13) of unstained material with the scanning transmission electron microscope (unpublished data).

The relatively clear density variation in the z-slices (Fig. 5) encouraged us to derive a model of the monomer (Fig. 9). In places where adjacent monomers touched, it was assumed that the lowest-density regions represented the contact areas. Although this does not unambiguously yield the correct

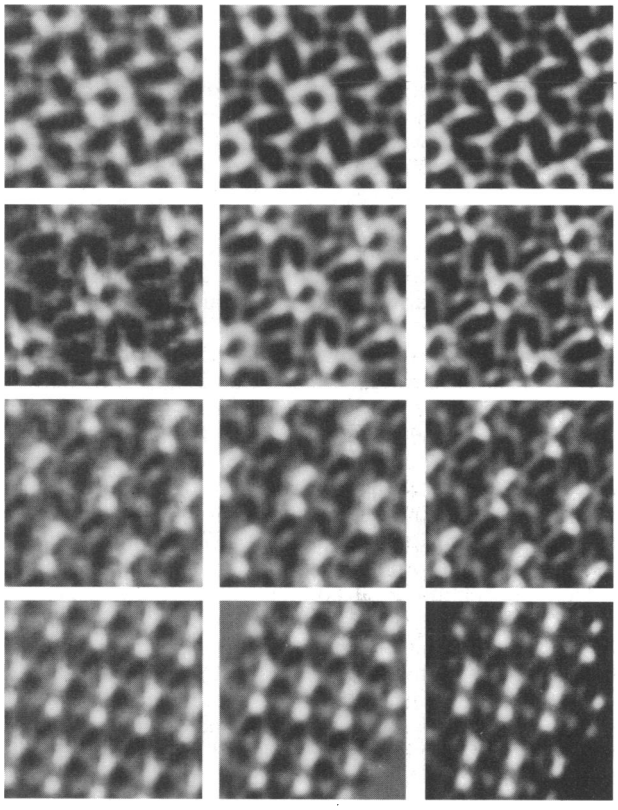

FIG. 4. Comparison of original averages of the tilted specimen (left column) and appropriate projections through the 3-D reconstruction nonthresholded (middle column) and thresholded (right column). The tilt angles were (from top to bottom) 6°, 40°, 58°, and 73°. With high tilts, only the central areas of the projections contain the complete information. The tilt axis azimuth with respect to the horizontal axis is 73°. The width of each image is 26 nm.

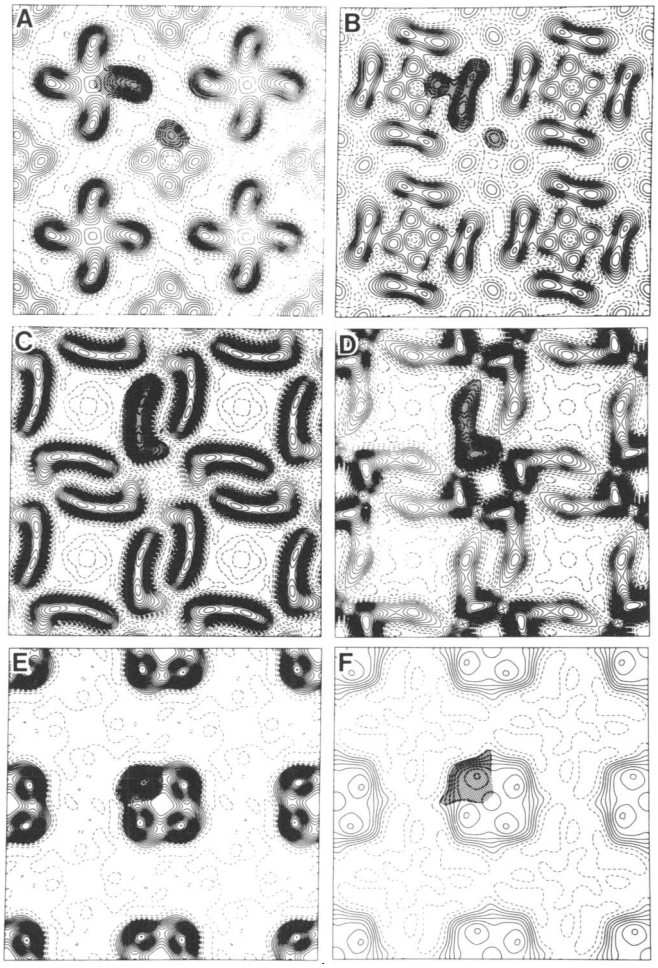

FIG. 5. Contour plots of selected horizontal sections (z-slices, sampled at 0.15-nm spacings) as follows: −2.6 nm (A), −1.2 nm (B), −0.3 nm (C), 0.3 nm (D), 1.2 nm (E), and 2.5 nm (F) from the central plane. Layer A shows the spurs (minor tetramer) at the subsidiary fourfold symmetry axes, layers B to D show the arm domain, and layers D to F show the core domain (major tetramer) of the S-layer. The core appears to be flattened (F) due to adsorption artifacts. The domains as extracted for modeling the putative monomer shown in Fig. 9 are emphasized.

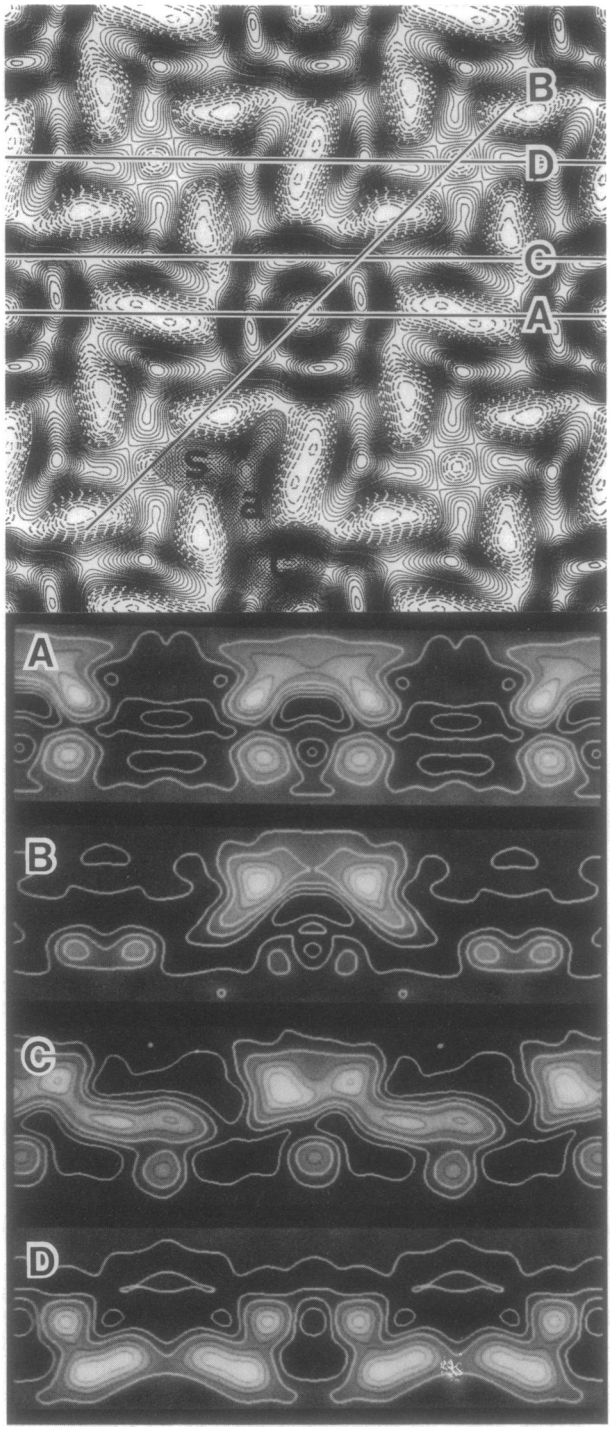

FIG. 6. Contour plot of a projection through the 3-D reconstruction along the z-axis. The shape of the putative monomer is emphasized and the core (c), arm (a), and spur (s) domains are marked. The lines indicate the positions of the vertical sections displayed below. The core of the S-layer is oriented towards the top and the spurs towards the bottom of the images. The size of each section is 26 by 8 nm.

molecular boundaries, the model of the putative monomer in Fig. 9 clearly illustrates the multidomain structure of the S-layer protein (maximum length, 10 nm). Estimates of the partial masses of the several domains are (assuming 115 kDa for the monomer): core domain, 40 to 50 kDa; arm domain without the thickening, i.e., part of the spur, 45 to 55 kDa; and the whole spur, ca. 20 to 25 kDa. The minor globular mass at the outer surface of the core occupies less than 10 kDa.

Assessment of the secondary structure. The IR spectrum, particularly in the amide I and II regions between 1,720 and 1,480 cm^{-1}, may be used as a diagnostic tool for protein secondary-structure determination (21); it is especially powerful in determining β-structure composition. The peak position of the amide I band at 1,640 cm^{-1} (Fig. 10) is indicative of an appreciable amount of β-structure in the S-layer protein; the band shape analysis yields a β-structure content of 37 ± 5%. The average length of β-strands may be estimated from the precise position of the band assigned to the β-structure (21). The position at 1,638 cm^{-1} corresponds to an average length of ca. 7 amino acid residues per β-strand. If we assume 0.35 nm to be the periodicity along the polypeptide chain (15), the average length of β-strands would be 2.5 nm. No attempts have been made to assess the portion of α-helix conformation. The strong component at 1,655 cm^{-1} and the peak position of the amide II band at 1,530 cm^{-1}, however, suggest that the α-helix content is low and that the remainder is largely in a random coil conformation.

DISCUSSION

The structure of the S-layer of *S. ureae* as revealed by 3-D reconstruction has proved to be more complex than might be anticipated from projections only. The reconstruction shows a clear domain structure. The surfaces are characteristically different, confirming the findings with low stain levels, which emphasize either the inner or the outer surface (33), and with heavy-metal-shadowed preparations (13a). The comparison of 3-D structures of different S-layers will provide valuable information concerning structural domains, conservative and variable features, etc., which should provide clues concerning their function. However, it has been shown (2) that two major artifacts may give rise to problems in interpreting and comparing 3-D reconstructions (for a more detailed discussion, see Baumeister and Engelhardt, in press). First, the layer protein may become distorted upon adsorption to the carbon support. Some flattening has been observed with the core of the *S. ureae* S-layer, but apparently none if the outer surface of the layer was adsorbed. The extent of distortions seems to vary greatly among S-layers (Baumeister and Engelhardt, in press). Due to flattening, the thickness of the *S. ureae* layer is likely to be slightly underestimated; it might be >7 nm rather than 6.6 nm. The second problem concerns artifacts created by missing information due to limited tilting (the missing-cone problem). A well-known, although occasionally disregarded, consequence is elongation of structures in the z-direction, which becomes dramatic if tilting is restricted to angles much below 60° (2, 13a). Accordingly, 3-D reconstructions of the S-layers of "*Synechocystis*" sp. (20) and *Chlamydia trachomatis* (10) with maximum tilt angles of 49° and 50°, respectively, suggest the layers to be very thick (13 to 14 nm). Probably more serious, however, is the problem of the artifacts (clutter) that may create spurious "masses" in the 3-D reconstruction (2, 13a). The pore of the S-layer of *S. ureae* appeared to be completely closed if tilting was restricted to 60°. This observation may be of particular importance if the diameters of pores are small or close to the resolution limit. Whether the pore of the *S. ureae* S-layer is

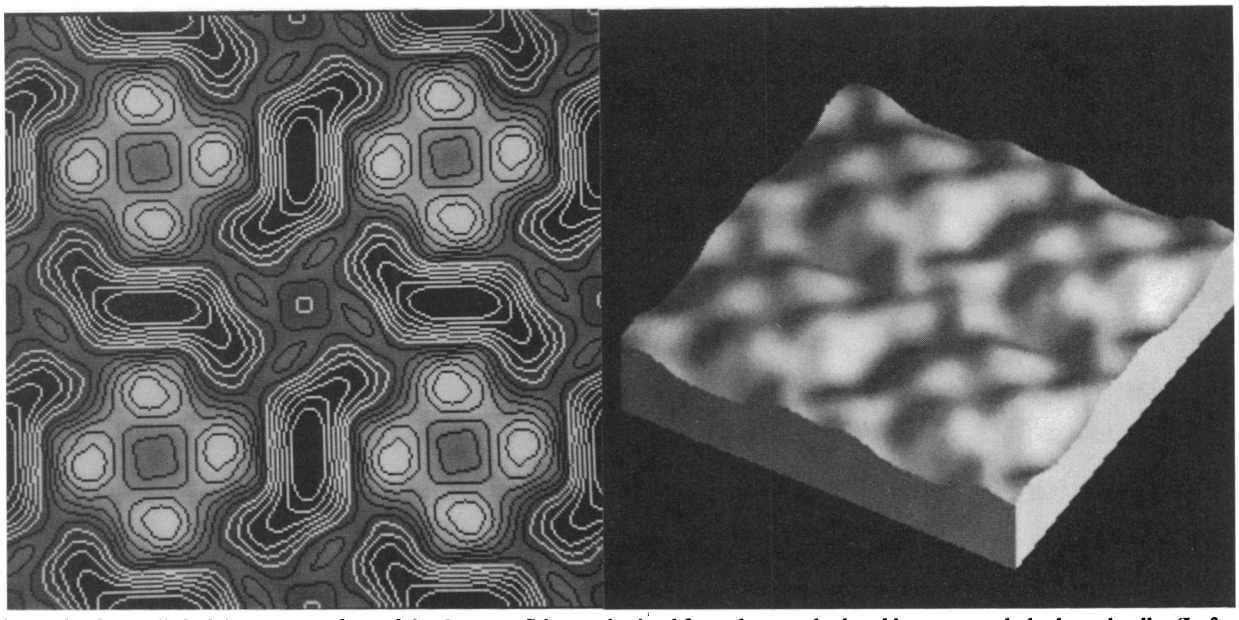

FIG. 7. Surface relief of the outer surface of the *S. ureae* S-layer obtained from deep-etched and heavy-metal-shadowed cells. (Left panel) The contoured projection shows the central (small) tetramer of the core and the prominent masses of the arm domains. It should be noted that the contour lines represent the relief heights. (Right panel) View of the outer surface of the S-layer.

closed (due to the missing cone effect or to structural distortions upon adsorption) cannot yet be determined; however, it may be that the opening is too small to be resolved clearly at the resolution achieved.

S-layers can be classified according to the scheme of Baumeister et al. (2) with respect to the symmetry, the locations of the major domain, and the connectivities. The notation M_nC_m describes a structure in which the heavier domains of the molecules form a massive (M) core around the *n*-fold symmetry axis while the lighter domains provide connectivity (C) across the *m*-fold symmetry axis. Accordingly, the *S. ureae* S-layer is classified as an $M_4C_{2,4}$ type since the connections at the twofold and subsidiary fourfold symmetry axes are of similar "strength." Few of the tetragonal S-layers (31) are sufficiently characterized to allow classification. The S-layers of the closely related species *S. ureae* and *B. sphaericus* (14, 24) can be classified in the same category. The layers of *Bacillus polymyxa* (7) and *Clostridium thermosaccharolyticum* (11), assigned as M_4C_2 types, appear to be similar to each other but differ significantly from the *S. ureae* S-layer, as far as it can be judged from 2-D averages. The lattice constants are smaller (10 and 11.5 nm, respectively), most of the mass is confined around the major fourfold symmetry axis, and the arms are shorter. *B. polymyxa* and the clostridia are less closely related to *S. ureae* than *B. sphaericus* (32). The tetragonal

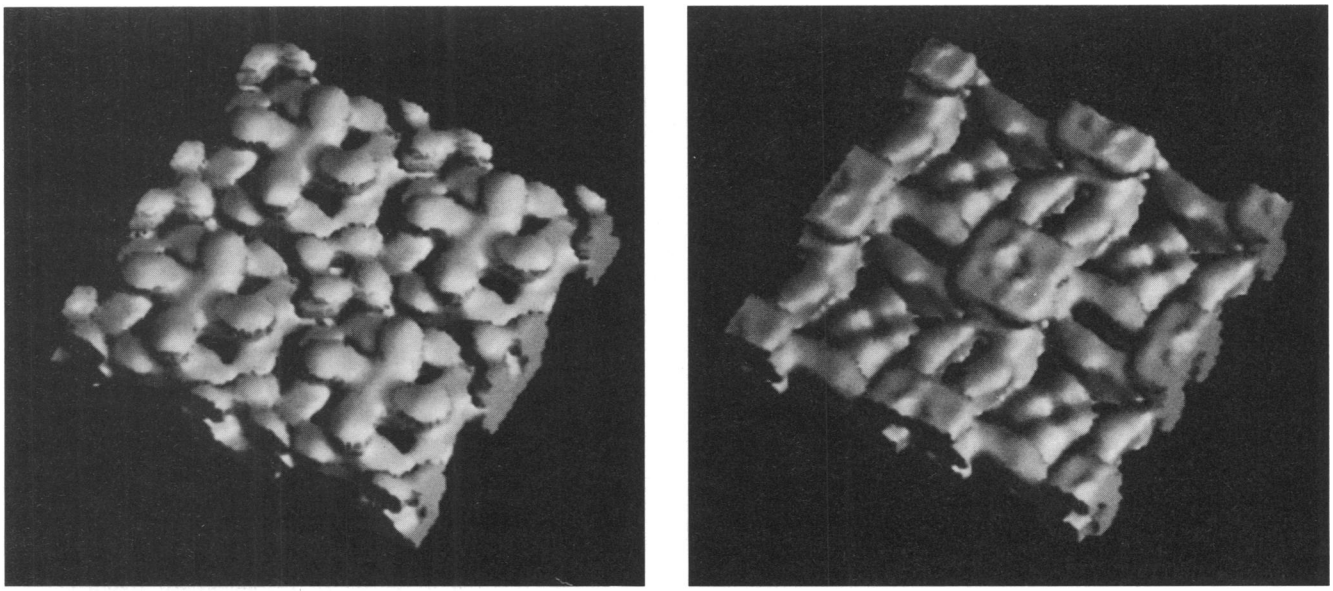

FIG. 8. 3-D representation of the reconstruction obtained by surface shading. Views of the outer surface (left) and the inner surface (right) are shown. Lattice constant, 12.9 nm.

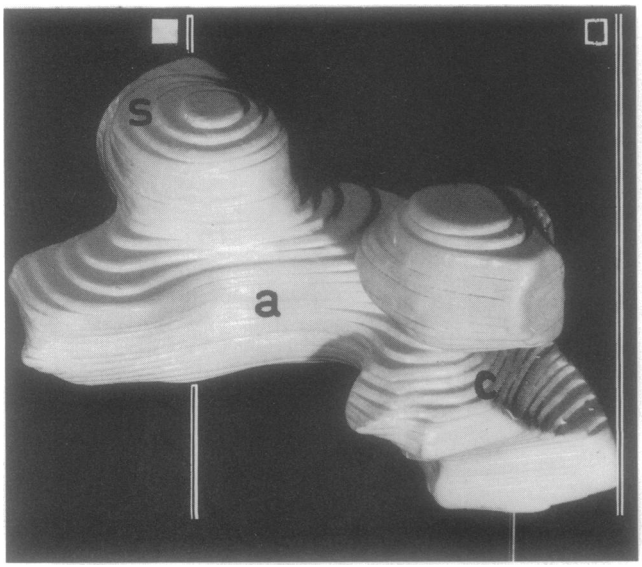

FIG. 9. Wooden model of the putative monomer of the S-layer: view of the outer surface with the core region to the right. The major (■) and subsidiary (□) fourfold symmetry axes, as well as the core (c), arm (a), and spur (s) domains, are indicated.

layers of the gram-negative species *Pseudomonas avenae* (35) and *P. acidovorans* (9) show a cobblestone pattern without clear domains and connectivities that is grossly different from those of other S-layers. There are apparently no features shared by the 3-D structures of the *P. acidovorans* and *S. ureae* layers.

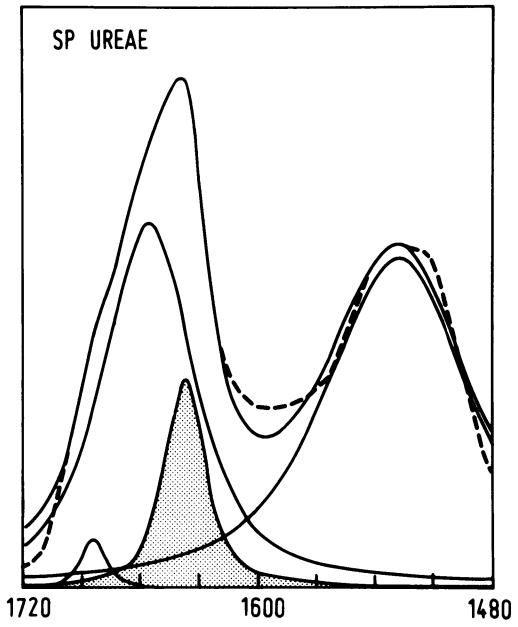

FIG. 10. IR spectrum of the S-layer in the range between 1,720 and 1480 cm^{-1} showing the amide I and II regions. Dotted line, Original absorption curve; continuous lines, deconvoluted (and superposed) bands. The (relative) area under the hatched band is proportional to the amount of β-structure in the protein.

It begins to emerge that S-layers have some structural principles in common: the outer surfaces appear to have a highly variable structure, clearly visible already on the level of domain structures, whereas the parts of the layer directed towards the interior of the cell are much more conservative. The layers of *S. ureae* and *B. sphaericus*, being almost identical in unit cell size and topology (22), show significant differences on the smooth faces corresponding to the outer surface. The core which is located towards the cell making contact with the peptidoglycan appears to be almost congruent in the 3-D reconstructions of *S. ureae* and *B. sphaericus* (22). Similar observations have been made with other (hexagonal) S-layers, e.g., of *Deinococccus radiodurans* (2), *Acetogenium kivui* (M. Rasch and W. Baumeister, unpublished data), and *Clostridium thermohydrosulfuricum* (18a). The outer surfaces frequently show large funnel-like openings of the pores, but appear to be more variable than the inner surfaces; this either indicates a weaker selection for a certain structure or reflects species-specific functions of S-layers related to the structure of the outer surface. The regular and individual surface structure of the exposed S-layers may well be suited to mediating specific cell-cell contacts. We have, in fact, observed that isolated fragments of the *S. ureae* S-layer spontaneously associate, such that the unit cells are precisely in register and the aligned pores form continuous channels across the two sheets (Engelhardt and Baumeister, unpublished data). According to a hypothesis of W. Baumeister and R. Hegerl (FEMS Microbiol. Lett., in press), such bacterial "connexons," if they occur in vivo, could be involved in the exchange of genetic material.

Apart from some equivalence in the domain structure, S-layers appear to have remarkably similar secondary-structure compositions. The proteins of *D. radiodurans* (4), *A. kivui* (M. Rasch and W. Baumeister, unpublished data), *S. ureae*, and *Azotobacter vinelandii* (6) show approximately equal portions of β-structure and, presumably, small amounts of α-helix. The correlation of secondary structure with certain domains, however, remains to be established. It is worth mentioning here that the S-layer of the archaebacterium *Sulfolobus acidocaldarius* (19) and the cell sheath of *Methanospirillum hungatii* (34) were also found to have appreciable amounts of β-structure.

More 3-D studies, as well as information on the primary protein structures, are required to establish structural relationships among S-layers and to shed some light on their evolution. The closely related species *S. ureae* and *B. sphaericus* ($S_{AB} > 0.6$) are particularly suited for investigating the species-specific features and differences of structurally similar S-layers. A more detailed study comparing the S-layers and their proteins is in preparation.

ACKNOWLEDGMENTS

We thank U. Jakubowski for determining the lattice constant, C. L. F. Woodcock for critically reading the manuscript, and Ute Santarius for excellent technical assistance.

LITERATURE CITED

1. **Aebi, U., P. R. Smith, J. Dubochet, C. Henry, and E. Kellenberger.** 1973. A study of the structure of the T-layer of *Bacillus brevis*. J. Supramol. Struct. **1**:498–522.
2. **Baumeister, W., M. Barth, R. Hegerl, R. Guckenberger, M. Hahn, and W. O. Saxton.** 1986. The three-dimensional structure of the regular surface layer (HPI-layer) of *Deinococcus radiodurans*. J. Mol. Biol. **187**:241–253.
3. **Baumeister, W., B. Emde, G. Flaskamp, M. Hahn, and R. Rachel.** 1981. Fine structure of a bacterial cell envelope protein: the RS-layer of *Sporosarcina ureae*. Naturwissenschaften

67:626–627.
4. **Baumeister, W., F. Karrenberg, R. Rachel, A. Engel, B. Ten Heggeler, and W. O. Saxton.** 1982. The major cell envelope protein of *Micrococcus radiodurans* (R1). Structural and chemical characterization. Eur. J. Biochem. **125**:535–544.
5. **Beveridge, T. J.** 1979. Surface arrays on the wall of *Sporosarcina ureae*. J. Bacteriol. **139**:1039–1048.
6. **Bingle, W. H., J. L. Doran, and W. J. Page.** 1986. Characterization of the surface layer protein from *Azotobacter vinelandii*. Can. J. Microbiol. **32**:112–120.
7. **Burley, S. K., and R. G. E. Murray.** 1983. Structure of the regular surface layer of *Bacillus polymyxa*. Can. J. Microbiol. **29**:775–780.
8. **Chalcroft, J. P., and C. L. Davey.** 1984. A simply constructed extreme-tilt holder for the Philips eucentric goniometer stage. J. Microsc. (Oxford) **134**:41–48.
9. **Chalcroft, J. P., H. Engelhardt, and W. Baumeister.** 1986. Three-dimensional structure of a regular surface layer from *Pseudomonas acidovorans*. Arch. Microbiol. **144**:196–200.
10. **Chang, J.-J., K. Leonard, T. Arad, T. Pitt, Y.-X. Zhang, and L.-H. Zhang.** 1982. Structural studies of the outer envelope of *Chlamydia trachomatis* by electron microscopy. J. Mol. Biol. **161**:579–590.
11. **Crowther, R. A., and U. B. Sleytr.** 1977. An analysis of the fine structure of the surface layers from two strains of *Clostridia*, including correction for distorted images. J. Ultrastruct. Res. **58**:41–49.
12. **Deatherage, J. F., K. A. Taylor, and L. A. Amos.** 1983. Three-dimensional arrangement of the cell wall protein of *Sulfolobus acidocaldarius*. J. Mol. Biol. **167**:823–852.
13. **Engel, A.** 1982. Mass determination by electron scattering. Micron **13**:425–436.
13a. **Engelhardt, H., W. O. Saxon, and W. Baumeister.** 1986. 3-D reconstruction of a regular bacterial surface layer: effects of limited tilting and preparation conditions, p. 168–169. *In* G. W. Bailey (ed.), Proceedings of the 44th Annual Meeting of the Electron Microscopy Society of America. San Francisco Press, Inc., San Francisco.
14. **Fox, G. E., E. Stackebrandt, R. B. Hespell, J. Gibson, J. Maniloff, T. A. Dyer, R. S. Wolfe, W. E. Balch, R. S. Tanner, L. J. Magrum, L. B. Zablen, R. Blakemore, R. Gupta, L. Bonen, B. J. Lewis, D. A. Stahl, K. R. Luehrsen, K. N. Chen, and C. R. Woese.** 1980. The phylogeny of prokaryotes. Science **209**:457–463.
15. **Fraser, R. D. B., and T. P. MacRae.** 1973. Conformation in fibrous proteins. Academic Press, Inc., New York.
16. **Fraser, R. D. B., and E. Suzuki.** 1973. The use of least squares in data analysis, p. 301–355. *In* S. J. Leach (ed.), Physical principles and techniques of protein chemistry, part C. Academic Press, Inc., New York.
17. **Glaeser, R. M., J. S. Jubb, and R. Henderson.** 1985. Structural comparison of native and deoxycholate-treated purple membrane. Biophys. J. **48**:775–780.
18. **Guckenberger, R.** 1985. Surface reliefs derived from heavy-metal-shadowed specimens: Fourier space techniques applied to periodic objects. Ultramicroscopy **16**:357–370.
18a. **Hegerl, R., Z. Cejka, and W. Baumeister.** 1986. A bacterial S-layer: separation of double lattices, correlation averaging, and 3-D reconstruction, p. 148–149. *In* G. W. Bailey (ed.), Proceedings of the 44th Annual Meeting of the Electron Microscopy Society of America. San Francisco Press, Inc., San Francisco.
19. **Inatomi, K.-I., M. Ohba, and T. Oshima.** 1983. Chemical properties of proteinaceous cell wall from an acido-thermophile, *Sulfolobus acidocaldarius*. Chem. Lett. **8**:1191–1194.
20. **Karlsson, B., T. Vaara, K. Lounatmaa, and H. Gyllenberg.** 1983. Three-dimensional structure of the regularly constructed surface layer from *Synechocystis* sp. strain CLII. J. Bacteriol. **156**:1338–1343.
21. **Kleffel, B., R. M. Garavito, W. Baumeister, and J. P. Rosenbusch.** 1985. Secondary structure of a channelforming protein: porin from *E. coli* outer membranes. EMBO J. **4**:1589–1592.
22. **Lepault, J., N. Martin, and K. Leonard.** 1986. Three-dimensional structure of the T-layer of *Bacillus sphaericus* P-1. J. Bacteriol. **168**:303–308.
23. **Lepault, J., and T. Pitt.** 1984. Projected structure of unstained, frozen-hydrated T-layer of *Bacillus brevis*. EMBO J. **3**:101–105.
24. **Pechman, K. J., B. J. Lewis, and C. R. Woese.** 1976. Phylogenetic status of *Sporosarcina ureae*. Int. J. Syst. Bacteriol. **26**:305–310.
25. **Saxton, W. O.** 1985. Computer generation of shaded images of solids and surfaces. Ultramicroscopy **16**:387–394.
26. **Saxton, W. O., and W. Baumeister.** 1982. The correlation averaging of a regularly arranged bacterial cell envelope protein. J. Microsc. (Oxford) **127**:127–138.
27. **Saxton, W. O., W. Baumeister, and M. Hahn.** 1984. Three-dimensional reconstruction of imperfect two-dimensional crystals. Ultramicroscopy **13**:57–70.
28. **Shaw, P. J.** 1984. Constrained least-squares fitting of the lattice lines in three-dimensional reconstruction of monolayer crystals. Ultramicroscopy **14**:363–366.
29. **Shaw, P. J., G. J. Hills, J. A. Henwood, J. E. Harris, and D. B. Archer.** 1985. Three-dimensional architecture of the cell sheath and septa of *Methanospirillum hungatei*. J. Bacteriol. **161**:750–757.
30. **Sjögren, A., S. Hovmöller, G. Farrants, H. Ranta, M. Haapasalo, K. Ranta, and K. Lounatmaa.** 1985. Structures of two different surface layers found in six *Bacteroides* strains. J. Bacteriol. **164**:1278–1282.
31. **Sleytr, U. B., and P. Messner.** 1983. Crystalline surface layers on bacteria. Annu. Rev. Microbiol. **37**:311–339.
32. **Stackebrandt, E., and C. R. Woese.** 1981. The evolution of prokaryotes, p. 1–31. *In* M. J. Carlile, J. F. Collins, and B. E. B. Moseley (ed.), Molecular and cellular aspects of microbial evolution. Society for General Microbiology Ltd., symposium 32. Cambridge University Press, Cambridge.
33. **Stewart, M., and T. J. Beveridge.** 1980. Structure of the regular surface layer of *Sporosarcina ureae*. J. Bacteriol. **142**:302–309.
34. **Stewart, M., T. J. Beveridge, and G. D. Sprott.** 1985. Crystalline order to high resolution in the sheath of *Methanospirillum hungatei*: a cross-beta structure. J. Mol. Biol. **183**:509–515.
35. **Wells, B., R. W. Horne, B. M. Lund, and N. R. King.** 1983. The ultrastructure of *Pseudomonas avenae*. I. Paracrystalline surface layer and extracellular material. Micron **14**:11–28.